Available online at www.sciencedirect.com
SCIENCE DIRECT®
PERGAMON
Chaos, Solitons and Fractals 19 (2004) 151–161
CHAOS SOLITONS & FRACTALS
www.elsevier.com/locate/chaos

Analytical drift reconstruction for visco-elastic impact oscillators operating in periodic and chaotic regimes

Ekaterina Pavlovskaia *, Marian Wiercigroch

Centre for Applied Dynamics Research, School of Engineering and Physical Sciences, King's College, Aberdeen University, Aberdeen AB24 3UE, UK

Accepted 24 March 2003

Communicated by T. Kapitaniak

Abstract

An impact oscillator with a drift, which is important in many applications, is considered. The model accounts for the visco-elastic impacts and is capable to mimic the dynamics of a bounded progressive motion. To simplify the dynamic analysis a simple transformation decoupling the original co-ordinates is proposed. As the result the bounded oscillations can be studied separately from the drift as the drift does not influence the dynamics of the bounded system. On the contrary the drift depends on the bounded dynamics and can be reconstructed once the bounded oscillatory motion is determined. The accuracy of the analytical reconstruction allows to calculate even strange chaotic attractors. Evolutions of co-existing periodic and strange attractors were studied.

1. Introduction

Impacting oscillators have many applications (e.g. [1–5]) and their fundamental dynamic behaviour has been studied vigorously in the past (e.g. [6–12]) showing great complexity and sensitivity to the system parameters and the initial conditions. In most cases it is assumed that the impacting system or its elements oscillate around their equilibrium positions. If one poses a fundamentally important question 'What will happen to the complex dynamics of an impact oscillator if a simultaneous drift occurs?', the answer cannot be easily found in the published literature. Only recently this question has started to be addressed [13–17]. The simplest physical model with drift comprised of a mass loaded by a force having static and harmonic components, and a dry friction slider was studied in [13,14]. Despite of its simple structure, a very complex dynamics was revealed. The main result from that work was a finding that the best progression occurs when the system responds periodically. A more complicated model including the visco-elastic properties of the contact between the impacting mass and the frictional slider has been formulated and its equations of motion have been developed in [15]. In [16] this model was used to mimic dynamics of vibro-impact ground moling system, and it was shown that it reflects well both the dynamics of the vibro-impact system and the soil resistance characteristics. It was also found that the maximum progression is achieved when the responses switch from periodic to chaotic. To calculate periodic responses and to determine conditions when the periodicity is lost, a special semi-analytical method was developed in [17]. The method constructs a periodic response assuming that each period is comprised of a sequence of distinct phases for which analytical solutions are known. Based on this assumption a system of four piecewise linear first order differential equations is transformed to a system of nonlinear algebraic equations. It should be noted that in

* Corresponding author.
E-mail address: e.pavlovskaya@eng.abdn.ac.uk (E. Pavlovskaia).

0960-0779/04/$ - see front matter
doi:10.1016/S0960-0779(03)00128-0

all these studies the system co-ordinates are drifting away from the initial position and it makes the application of standard tools of nonlinear dynamics difficult. To overcome this difficulty a simple co-ordinate transformation is proposed in this paper, and analytical drift reconstruction for visco-elastic impact oscillators is developed.

The paper is organized as follows. In the next section, the description of the considered impact oscillator and equations of motion are given. These equations of motion are linear for each phase and their solutions are unbounded as the system drifts from the initial position. A simple co-ordinate transformation which allows to separate the bounded oscillatory motion from the drift is presented in the next section. In this section the solutions of the new equations of motion for each phase are also given. In Section 4 it is shown how to reconstruct a progressive motion of the system if the dynamics of the bounded system is known and this is illustrated by three examples. The accuracy of the proposed analytical method allows to reconstruct the chaotic strange attractor, which together with some nonlinear dynamics studies are discussed in Section 5.

2. Impact oscillator with drift

We consider a simple two degrees-of-freedom oscillator in nondimensional form, which is shown in Fig. 1. A mass m is driven by an external force f containing static b and dynamic $a\cos(\omega\tau+\varphi)$ components. The weightless slider has a linear visco-elastic pair of stiffness k and damping ratio 2ξ. As has been reported in [15] the slider drifts in stick-slip phases where the relative oscillations between the mass and the slider are bounded ranging from periodic to chaotic motion. Similarly to the stick-slip phenomena reported in [18,19], the progressive motion of the mass occurs when the force acting on the slider exceeds the threshold of the dry friction force d. x, z, v represent the absolute displacements of the mass, slider top and slider bottom, respectively. It is assumed that the model operates in a horizontal plane, or the gravitational force is compensated. At the initial moment $\tau=0$ there is a distance between the mass and the slider top called gap, g. The difference $(z+g)-x$ allows to monitor this distance in time. For the simplicity of the further analysis the dimensionless friction threshold force, d is set to 1 and for all numerical examples $\varphi=\pi/2$, $g=0.02$.

The considered system operates at the time in one of the following modes: *no contact*, *contact without progression*, and *contact with progression*. A detailed consideration of these modes and dimensional form of the equations of motion can be found in [15]. For the purpose of clarity a brief summary outlining how all particular phases of the dynamic responses were defined is given below.

No contact. If the distance between the mass and the slider top is greater than zero, $z+g-x>0$, then the mass and the slider top move separately. The motion of the mass is determined from:

$$x'=y,\quad y'=a\cos(\omega\tau+\varphi)+b, \tag{1}$$

where $'$ denotes $\mathrm{d}/\mathrm{d}\tau$. Equations of motion for the top and the bottom of the slider are

$$z'=-\frac{1}{2\xi}(z-v), \tag{2}$$

$$v'=0. \tag{3}$$

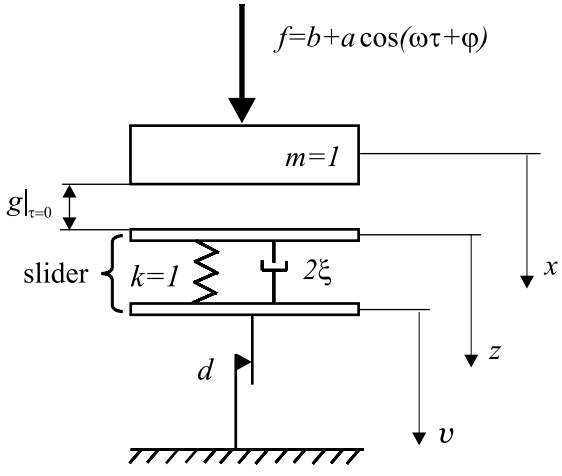

Fig. 1. Physical model of impact system with drift.

Contact without progression. This mode occurs when the distance between the mass and the slider top is equal to zero, i.e. $z+g-x=0$, and the force acting on the mass from the slider is greater than zero but smaller than the threshold of the dry friction force. This can be expressed as

$$0 < 2\xi z' + (z - v) < 1. \tag{4}$$

The mass and the slider top move together without progression, and the second equation of (1) gains additional elastic and viscous terms:

$$x' = y, \quad y' = -2\xi z' - (z - v) + a\cos(\omega\tau + \varphi) + b. \tag{5}$$

The velocity of the slider top is equal to the velocity of the mass, and the displacement of the slider top is in phase with the mass displacement but differs by gap, g

$$z' = x', \quad x = z + g. \tag{6}$$

When there is no progression, the bottom of the slider remains stationary, hence its velocity is equal to zero, $v' = 0$.

Contact with progression. When the distance between the mass and the slider top is equal to zero, $z+g-x=0$, and the force acting on the mass is greater than the threshold of dry friction force which can be described as

$$2\xi z' + (z - v) \geqslant 1, \tag{7}$$

the mass and the top and the bottom of the slider move together, and progression takes place. Equations of motion for the mass are

$$x' = y, \quad y' = a\cos(\omega\tau + \varphi) + b - 1. \tag{8}$$

The displacement and the velocity of the slider top are as before (see Eq. (6)). The velocity of the slider bottom can be calculated from the expression:

$$v' = z' + \frac{1}{2\xi}(z - v - 1). \tag{9}$$

3. Separation of bounded oscillatory motion from drift

The basic aim of the investigated system is to overcome the frictional force and move downwards. This means that the displacements of the mass and the slider are unbounded. In addition, the dynamics of this system is very complex ranging from different types of periodic motion to chaos [15]. These facts rise some difficulties in analysing the system dynamics in a standard way. In this paper we give a simple co-ordinates transformation, which resolves the problem of the motion unboundiness.

We introduce a new system of co-ordinates (p, q, v) instead of (x, z, v):

$$p = x - v, \quad q = z - v. \tag{10}$$

The main idea behind this transformation is to separate the oscillatory motion of the system from the drift. In fact in the new co-ordinates system p and q are displacements of the mass and the slider top relative to the current position of the slider bottom v. It will be demonstrated here that the introduction of the new co-ordinates allows to study a progressive motion shown in Fig. 2(a) as independent bounded oscillations depicted in Fig. 2(b) and dependent on them drift shown in Fig. 2(c).

The equations of motion for each phase can be rewritten as follow:

No contact

$$\begin{aligned} &p' = y, \quad y' = a\cos(\omega\tau + \varphi) + b, \quad \text{for } p < q + g, \\ &q' = -\frac{1}{2\xi}q, \quad v' = 0. \end{aligned} \tag{11}$$

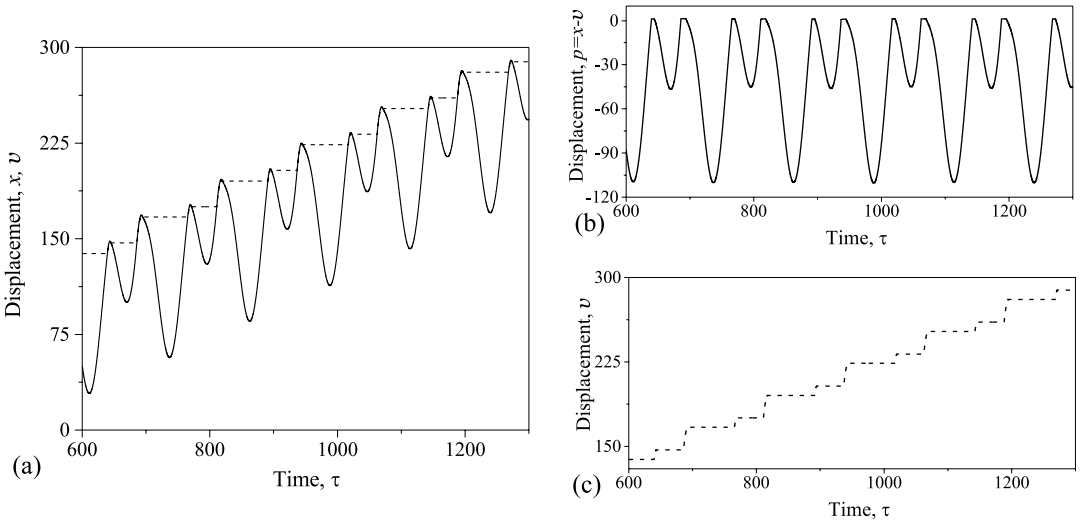

Fig. 2. Time histories of (a) drifting displacement of the mass (solid line) and the slider bottom (dash line); (b) bounded displacement of the mass $p = x - v$; and (c) progressive displacement of the slider bottom v.

Contact without progression

$$\begin{aligned} p' &= y, \\ y' &= -2\xi y - q + a\cos(\omega\tau + \varphi) + b, \quad \text{for } p = q + g \quad \text{and} \quad 0 < 2\xi y + q < 1, \\ q' &= y, \quad v' = 0. \end{aligned} \tag{12}$$

Contact with progression

$$\begin{aligned} p' &= -\frac{1}{2\xi}(q-1), \\ y' &= a\cos(\omega\tau + \varphi) + b - 1, \qquad \text{for } p = q + g \quad \text{and} \quad 2\xi y + q \geqslant 1, \\ q' &= -\frac{1}{2\xi}(q-1), \quad v' = y + \frac{1}{2\xi}(q-1). \end{aligned} \tag{13}$$

As can be clearly seen from Eqs. (11)–(13), the first three equations of each set describing the mass and slider top motions do not depend on the displacement of the slider bottom, v. This means that there is no influence of the progression v on the bounded system dynamics. On contrary the motion of the slider bottom depends on the mass velocity and the displacement of the slider top (see the last equation of (13)), hence the progression (drift) can be determined once the oscillatory mass and the slider top motions are known.

The equations of motion are linear for each phase, therefore the global solution can be constructed by joining the local solutions for each phase at the points of discontinuities. The set of initial values $(\tau_0; p_0, y_0, q_0)$ defines in which phase the system will operate. If $p_0 < q_0 + g$, it will be *no contact* phase. For $p_0 = q_0 + g$, it will be *contact without progression* phase if $0 < 2\xi y_0 + q_0 < 1$ or *contact with progression* phase if $2\xi y_0 + q_0 \geqslant 1$. The solutions for each phase are given below.

For *no contact* phase:

$$\begin{aligned} p(\tau) &= p_0 + y_0(\tau - \tau_0) + \frac{b}{2}(\tau - \tau_0)^2 \\ &\quad - \frac{a}{\omega^2}[\cos(\omega\tau + \varphi) - \cos(\omega\tau_0 + \varphi) + \omega(\tau - \tau_0)\sin(\omega\tau_0 + \varphi)], \\ y(\tau) &= y_0 + b(\tau - \tau_0) + \frac{a}{\omega}[\sin(\omega\tau + \varphi) - \sin(\omega\tau_0 + \varphi)], \\ q(\tau) &= q_0 \exp\left(-\frac{\tau - \tau_0}{2\xi}\right). \end{aligned} \tag{14}$$

For *contact without progression* phase:

$$\begin{aligned}
p(\tau) &= b + g + \exp(-\xi(\tau-\tau_0))\sqrt{C_1^2 + C_2^2}\sin\left(\sqrt{1-\xi^2}(\tau-\tau_0)+\beta\right) \\
&\quad + \frac{a}{\sqrt{(1-\omega^2)^2 + 4\xi^2\omega^2}}\sin(\omega\tau+\varphi+\alpha), \\
y(\tau) &= \exp(-\xi(\tau-\tau_0))\sqrt{C_1^2 + C_2^2}\sin\left(\sqrt{1-\xi^2}(\tau-\tau_0)+\delta\right) \\
&\quad + \frac{a\omega}{\sqrt{(1-\omega^2)^2 + 4\xi^2\omega^2}}\cos(\omega\tau+\varphi+\alpha), \\
q(\tau) &= b + \exp(-\xi(\tau-\tau_0))\sqrt{C_1^2 + C_2^2}\sin\left(\sqrt{1-\xi^2}(\tau-\tau_0)+\beta\right) \\
&\quad + \frac{a}{\sqrt{(1-\omega^2)^2 + 4\xi^2\omega^2}}\sin(\omega\tau+\varphi+\alpha),
\end{aligned} \tag{15}$$

where

$$C_1 = p_0 - b - g - \frac{a}{\sqrt{(1-\omega^2)^2 + 4\xi^2\omega^2}}\sin(\omega\tau_0+\varphi+\alpha), \tag{16}$$

$$C_2 = \frac{1}{\sqrt{1-\xi^2}}\left\{ y_0 + \xi(p_0 - b - g) - \frac{a\sqrt{\xi^2+\omega^2}}{\sqrt{(1-\omega^2)^2 + 4\xi^2\omega^2}}\sin(\omega\tau_0+\varphi+\alpha+\gamma)\right\}, \tag{17}$$

$$\alpha = \arctan\left(\frac{1-\omega^2}{2\xi\omega}\right),$$

$$\beta = \arctan\left(\frac{C_1}{C_2}\right),$$

$$\gamma = \arctan\left(\frac{\omega}{\xi}\right),$$

$$\delta = \arctan\left(\frac{-\xi C_1 + \sqrt{1-\xi^2}C_2}{-\sqrt{1-\xi^2}C_1 - \xi C_2}\right).$$

For *contact with progression* phase:

$$\begin{aligned}
p(\tau) &= g + 1 + (p_0 - g - 1)\exp\left(-\frac{\tau-\tau_0}{2\xi}\right), \\
y(\tau) &= y_0 + (b-1)(\tau-\tau_0) + \frac{a}{\omega}[\sin(\omega\tau+\varphi) - \sin(\omega\tau_0+\varphi)], \\
q(\tau) &= (q_0 - 1)\exp\left(-\frac{\tau-\tau_0}{2\xi}\right) + 1.
\end{aligned} \tag{18}$$

When the conditions corresponding to the current phase fail, the next phase begins, and the final displacements and velocity for the preceding phase define the initial conditions for the next one. The details of the semi-analytical method allowing to calculate the responses of the system using this idea are outlined in [17].

4. Reconstruction of progressive motion

As was mentioned before, the progression $v(\tau)$ can be calculated separately if the dynamics of the bounded system (p, y, q) is known (i.e. the sequence of the phases and the initial conditions for them). By solving the last equations of Eqs. (11)–(13) we have learnt that during the *no contact* and *contact without progression* phases the progression does not change its value and is equal to

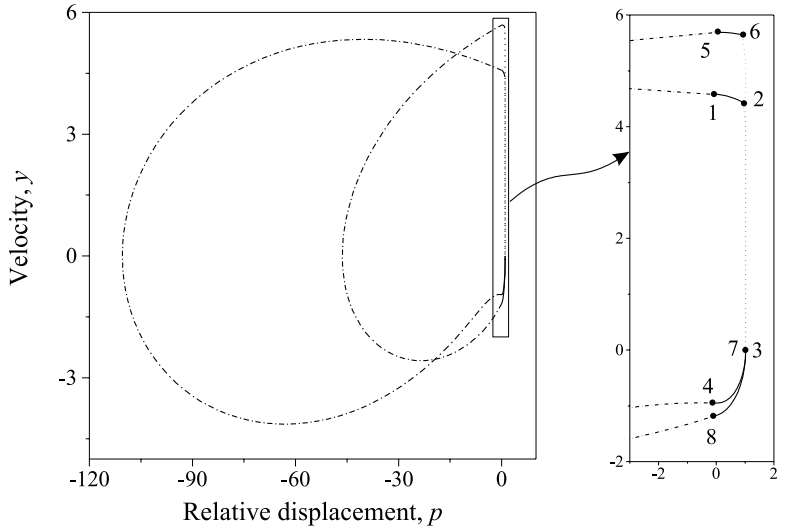

Fig. 3. Phase plane of a period two motion constructed for $a = 0.3$, $b = 0.1$, $\xi = 0.01$, $\omega = 0.1$. *No contact* phase is marked by dash and dotted lines, *contact without progression* phase—by solid lines and *contact with progression* phase—by dotted lines.

Table 1
Sequence of phases and corresponding initial conditions

Point	Phase	τ_0	p_0	y_0	q_0
1	Contact without progression	1142.28514	0.02	4.58005	0.0
2	Contact with progression	1142.48663	0.93131	4.43472	0.91131
3	Contact without progression	1146.21267	1.02	0.0	1.0
4	No contact	1147.60385	0.04328	−1.16404	0.02328
5	Contact without progression	1188.10028	0.02	5.68688	0.0
6	Contact with progression	1188.25661	0.90719	5.64034	0.88719
7	Contact without progression	1194.99997	1.02	0.0	1.0
8	No contact	1196.61048	0.03901	−0.95049	0.01901
1	Contact without progression	1267.97881	0.02	4.57225	0.0

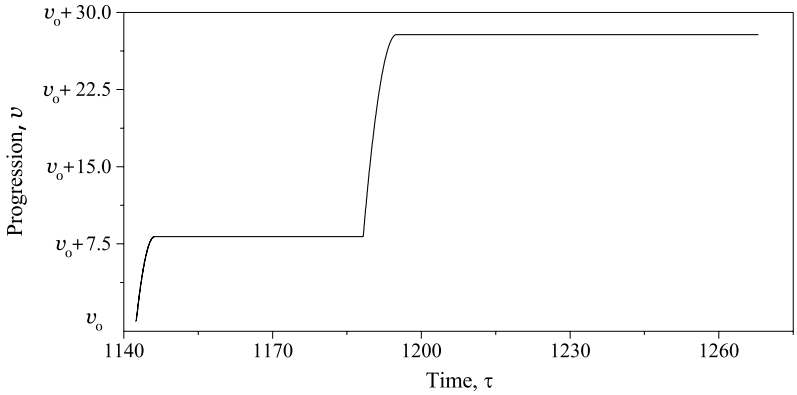

Fig. 4. Reconstructed progression using Table 1 and Eqs. (19) and (20); $a = 0.3$, $b = 0.1$, $\xi = 0.01$, $\omega = 0.1$.

$$v(\tau) = v_0. \tag{19}$$

During the *contact with progression* phase it can be calculated as

$$v(\tau) = v_0 + p_0 - g - 1 + (p_0 - g - 1)\exp\left(-\frac{\tau - \tau_0}{2\xi}\right) + y_0(\tau - \tau_0) + \frac{b-1}{2}(\tau - \tau_0)^2 - \frac{a}{\omega^2}[\cos(\omega\tau + \varphi) - \cos(\omega\tau_0 + \varphi) + \omega(\tau - \tau_0)\sin(\omega\tau_0 + \varphi)]. \tag{20}$$

To make the procedure of reconstruction of progressive motion clearer let us consider a numerical example. In Fig. 3 a phase plane of a period two motion is shown. Dash and dotted, solid and dotted lines denote *no contact*, *contact without progression* and *contact with progression* phases respectively. This phase portrait was constructed analytically using the data from Table 1, where a typical sequence of the different phases and corresponding to them initial conditions are listed. The values in Table 1 were calculated using the semi-analytical method developed for this system and outlined in [17]. The described portion of a complete table of initial conditions starts at the moment $\tau_0 = 1142.28514$,

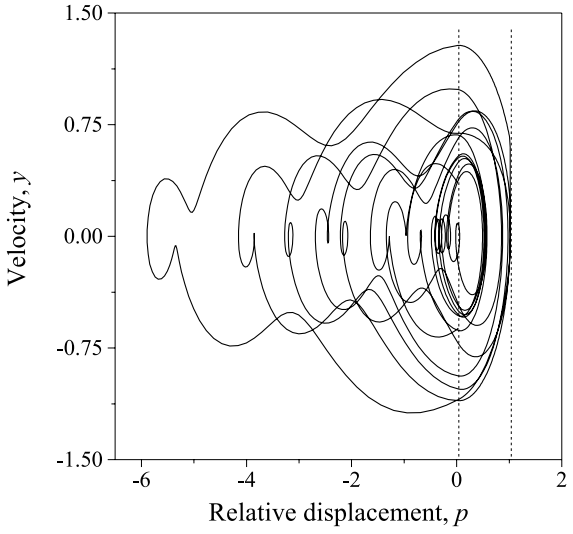

Fig. 5. Chaotic motion on the phase plane for $a = 0.3$, $b = 0.1$, $\xi = 0.01$, $\omega = 1.4$.

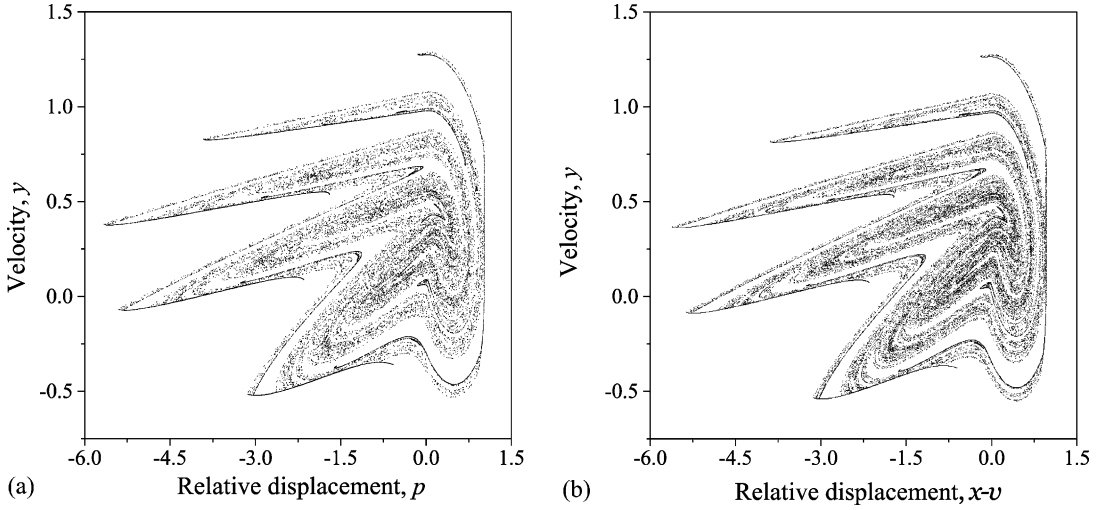

Fig. 6. Poincaré section for $a = 0.3$, $b = 0.1$, $\xi = 0.01$, $\omega = 1.4$; (a) calculated semi-analytically; (b) obtained by direct numerical integration.

when the *contact without progression* phase begins, and ends at $\tau_0 = 1267.97881$ after one period $T = 2T_{ext} = 2(2\pi/\omega)$. In this case one period of motion is comprised of eight phases commencing at points 1–8 depicted in the zoom-up of the stick-slip motion of Fig. 3. Having this data it is possible to reconstruct the progression of the system, which is shown in Fig. 4.

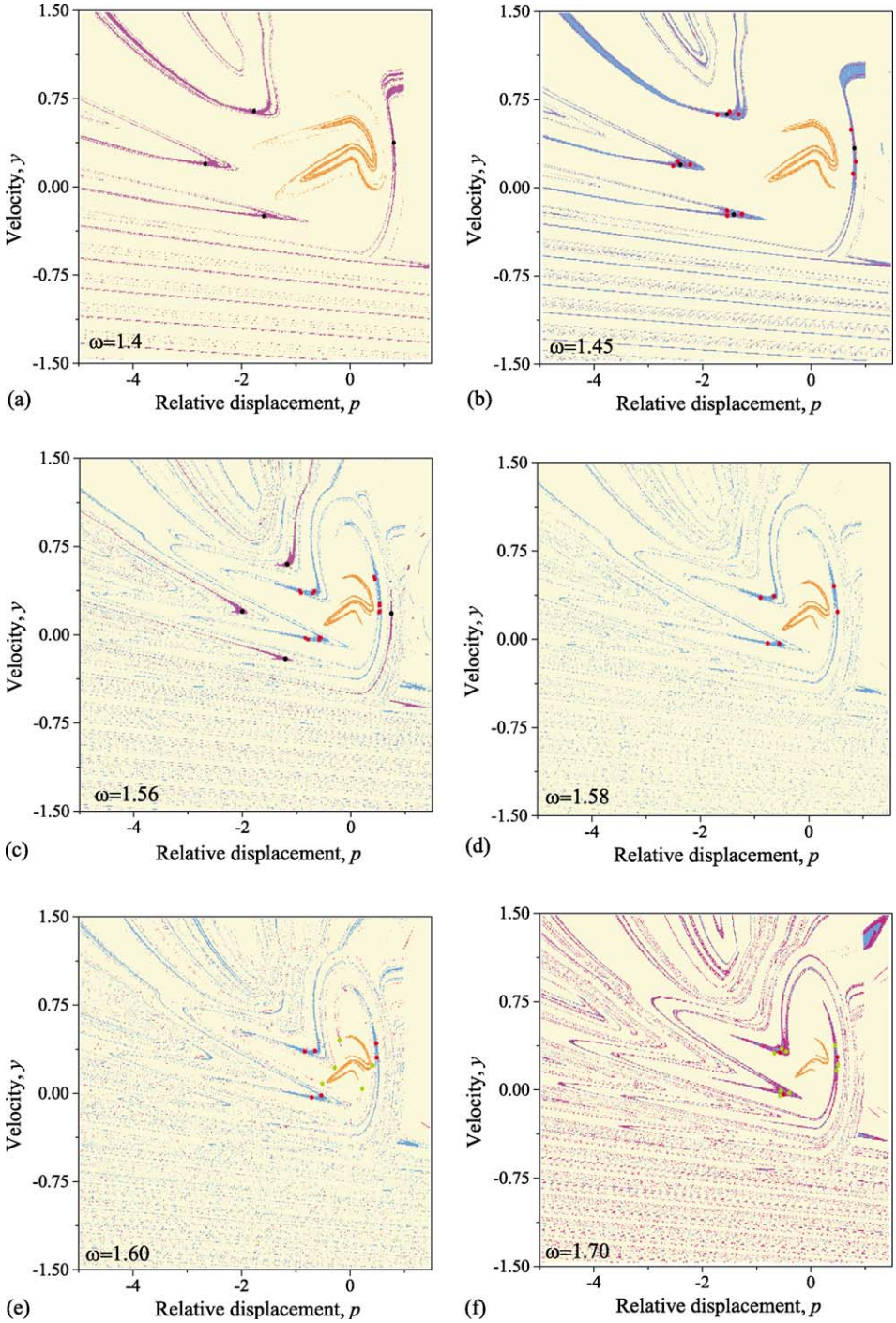

Fig. 7. Evolution of basins of attraction for $a = 0.3$, $b = 0.1$, $\xi = 0.1$; (a) $\omega = 1.4$, (b) $\omega = 1.45$, (c) $\omega = 1.56$, (d) $\omega = 1.58$, (e) $\omega = 1.60$ and (f) $\omega = 1.70$.

It can be clearly seen from Fig. 3 that at $p < 0.02$ system operates in *no contact* phase. The reason for this is that the condition for this phase is $p < g + q$ and q is always positive (the top of the slider is not able to move in opposite way to the progression). For *contact with progression* phase the velocity of the mass y is always positive and the displacement of the mass p is very close to 1.02 as $\exp(-(\tau - \tau_0)/2\xi)$ rapidly tends to 0.

Using the same procedure any dynamic response can be calculated. In Fig. 5 a phase portrait of chaotic motion ($a = 0.3$, $b = 0.1$, $\xi = 0.01$, $\omega = 1.4$) for 40 periods of external excitation is shown. The parts of the curve which are located on the left from left dash line, account for the *no contact* phase, while those between two dash lines for the *contact without progression* phase, and finally the ones which coincide with right dash line, denote the *contact with progression* phase.

The presented method of constructing tables of various phases of motion allows to calculate even chaotic responses. Since motion within a particular phase is described analytically with the initial conditions determined from a set of nonlinear algebraic equations [17], the accuracy of this method is high. For example, Poincaré sections shown in Fig. 6 give a comparison between strange attractors calculated by our semi-analytical method and by a direct numerical integration using *Dynamics* package [20]. More insight in the investigated system dynamics is given below.

5. Nonlinear dynamics analysis

The proposed co-ordinate transformation allows to study dynamics of the systems with drift in the same way as systems with bounded oscillations. Once the drift is subtracted from the oscillatory motion the cell-to-cell mapping method [21] can be deployed to find co-existing attractors and their basins. Evolution of the strange attractor and co-existing periodic orbits under increasing frequency ω is shown in Fig. 7 for $a = 0.3$, $b = 0.1$, $\xi = 0.1$. The presented basins of attractions have been constructed using Dynamics package [20] adopting the following colour coding. The strange chaotic attractor and its basin are marked in orange and yellow respectively. The period four motion and its basin are coloured in black and purple. Red colour marks the attractor for blue basin, and green colour marks the attractor for pink basin. All presented cases feature fractal boundaries of attractions. For larger ω there is noticeable increase in fractality of the basins or erosion of basin of attraction (see [22] for example).

As can be seen from Fig. 7 co-existence of two (Fig. 7a and d) and three (Fig. 7b, c, e and f) attractors were found for this set of parameters. These attractors can be clearly seen in Figs. 8 and 9, where they are separated. Phase planes are drawn to show the shape of periodic orbits and Poincaré maps are constructed for chaotic strange attractors. At $\omega = 1.4$ period four orbit (Fig. 8a) and strange attractor (Fig. 8b) were determined. As basins of attractions of these attractors are moving significantly under changing frequency, appropriate corrections have to be made to follow the structural changes of these attractors (bifurcations). The difficulty of following periodic orbit is demonstrated in Fig. 10, where two bifurcation diagrams are used to monitor period four attractor shown in Figs. 7a–c and 8a. The first of them (Fig. 10a) is constructed taking into account the changes of the basin of attraction by appropriately choosing initial conditions obtaining eventually a real picture of the attractor evolution. The second bifurcation diagram (Fig. 10b) is calculated without correction of initial conditions resulting in appearance of false bifurcations. This is due to inappropriate initial conditions to follow period four. For example, there is no bifurcation of period four into period 12 at $\omega \approx 1.445$. As can be clearly seen from Fig. 7b these two attractors co-exist for $\omega = 1.45$, and their basins are strongly intertangled. With the frequency being increased period twelve attractor disappears, a new chaotic attractor (coloured

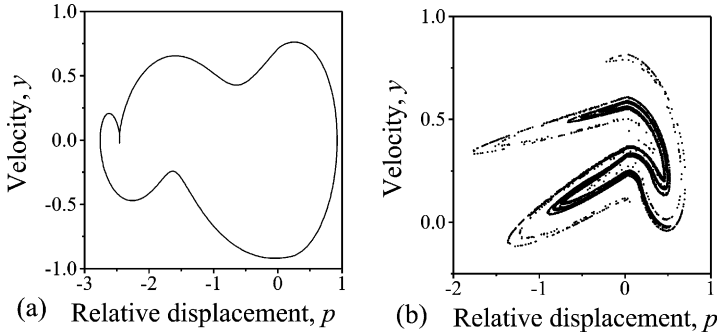

Fig. 8. Coexisting attractors for $a = 0.3$, $b = 0.1$, $\xi = 0.1$, $\omega = 1.4$ (see Fig. 7a): (a) phase plane for period four attractor and (b) Poincaré section for strange attractor.

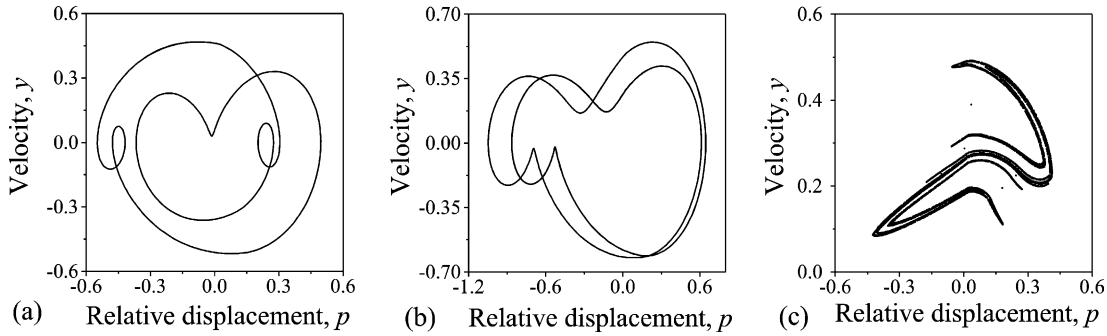

Fig. 9. Coexisting attractors for $a = 0.3$, $b = 0.1$, $\xi = 0.1$, $\omega = 1.6$ (see Fig. 7e): phase planes for (a) period five and (b) period six attractors and (c) Poincaré section for strange attractor.

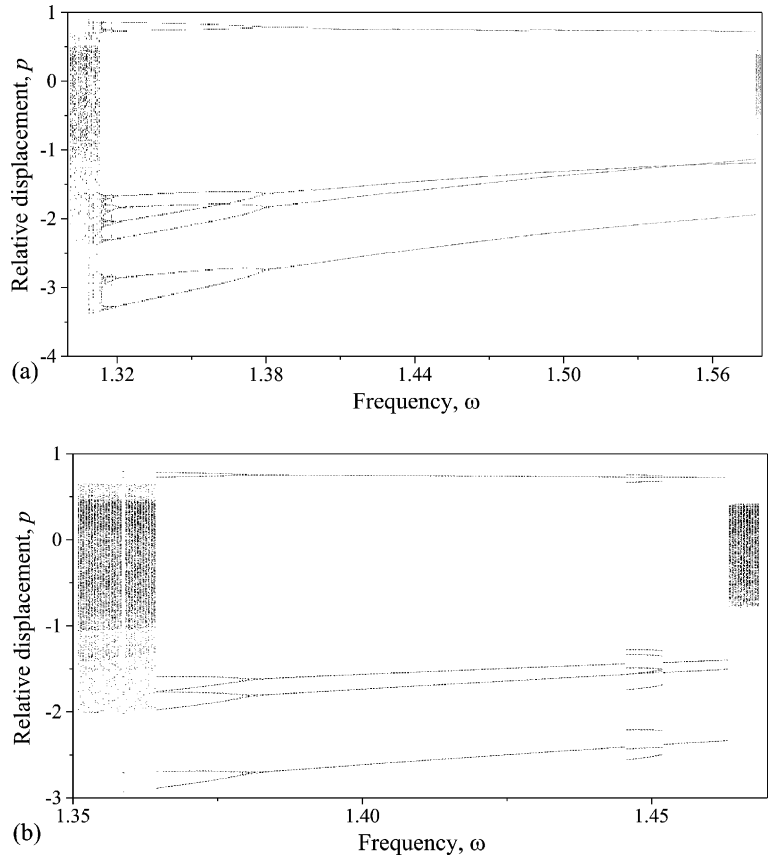

Fig. 10. Bifurcation diagram $p = f(\omega)$ for $a = 0.3$, $b = 0.1$, $\xi = 0.1$ for period four attractor (a) with initial conditions correction and (b) without it.

in red) emerges, and at $\omega = 1.56$ the basins of this new attractor and the period four are easily distinguished as can be seem from Fig. 7c. At $\omega \approx 1.571$ the above mentioned chaotic motion bifurcates through cascade of subcritical period-doubling bifurcations into period six. At $\omega \approx 1.5757$ the period four attractor disappears and its basin of attraction merges with the basin of the strange attractor. Thus the only two attractors co-exist at $\omega = 1.58$ as shown in Fig. 7d. Then a new attractor emerges, and at $\omega = 1.6$ we have co-existence of two periodic (period five and period six) and strange attractors (Fig. 7e). These coexisting attractors are shown in Fig. 9 as phase planes and Poincaré map. Finally

the period six attractor undergoes a subcritical bifurcation into a period three at $\omega \approx 1.6395$, and at $\omega = 1.7$ we have co-existence of the period three, a new period nine and the strange attractors as shown in Fig. 7f.

6. Conclusions

In this paper, an impact oscillator with a drift is considered. The dynamics of this system is very complex ranging from different types of periodic motion to chaos. The solutions of the equations of motion constructed for each phase allow to calculate dynamic responses exactly, i.e. without necessity of numerical integration. The global solution is obtained by joining together the local solutions for different phases in the points of discontinuities, which are roots of the resulting nonlinear algebraic equations. To simplify the dynamic analysis of this system even further, a co-ordinate transformation has been proposed. The main idea behind this transformation is very simple, i.e. to monitor the displacements of the system elements relatively to the progression of the system (see Eqs. (11)–(13)). As the result the bounded system oscillations can be studied separately from the drift (progression) as the drift does not influence the dynamics of the bounded system. On the contrary the drift of the system depends on the bounded dynamics and can be determined once the bounded oscillatory motion is known. The proposed co-ordinate transformation allows to study system with drift as a bounded dynamical system, therefore the standard tools of nonlinear dynamics analysis can be used. The evolution of the basins of attractions was investigated showing co-existence of three different attractors having fractal boundaries.

Acknowledgement

This research was supported by EPSRC under the grants GR/N16341/01 and GR/R85556/01.

References

[1] Goyda H, Teh C. A study of the impact dynamics of loosely supported heat exchanger tubes. J Press Vessel Technol 1989;111:394–401.
[2] Wiercigroch M, Neilson RD, Player MA. Material removal rate prediction for ultrasonic drilling of hard materials using impact oscillators approach. Phys Lett A 1999;259:91–6.
[3] Woo K-C, Rodger AA, Neilson RD, Wiercigroch M. Application of the harmonic balance method to ground moling machines operating in periodic regimes. Chaos, Solitons & Fractals 2000;11:2515–25.
[4] Astashev VK, Babitsky VI. Ultrasonic cutting as a nonlinear (vibro-impact) process. Ultrasonics 1998;36:89–96.
[5] Tung PC, Shaw SW. The dynamics of an impact print hammer. J Vib Acoust 1988;110(2):193–200.
[6] Kobrinskii AE. Dynamics of mechanisms with elastic connections and impact systems. London: ILIFFE Books Ltd; 1969.
[7] Peterka F. Laws of impact motion of mechanical systems with one degree of freedom. Acta Technica ČSAV, Part I—Theoretical analysis of n-multiple (1/n)-impact motions, vol. 4, 1974. p. 462–73.
[8] Thompson JMT, Ghaffari R. Chaotic dynamics of an impact oscillator. Phys Rev A 1983;27:1741–3.
[9] Shaw SW, Holmes PJ. A periodically forced piecewise linear oscillator. J Sound Vib 1983;90:129–55.
[10] Foale S, Bishop SR. Dynamic complexities of forced impacting systems. Philos Trans R Soc London A 1992;338:547–56.
[11] Chin W, Ott E, Nusse HE, Grebogi C. Grazing bifurcations in impact oscillators. Phys Rev E 1994;50:4427–44.
[12] Banerjee S, Grebogi C. Border collision bifurcations in two-dimensional piecewise smooth maps. Phys Rev E 1999;59:4052–61.
[13] Krivtsov AM, Wiercigroch M. Dry friction model of percussive drilling. Meccanica 1999;34:425–34.
[14] Krivtsov AM, Wiercigroch M. Penetration rate prediction for percussive drilling via dry friction model. Chaos, Solitons & Fractals 2000;11:2479–85.
[15] Pavlovskaia E, Wiercigroch M, Grebogi C. Modeling of an impact system with a drift. Phys Rev E 2001;64:056224.
[16] Pavlovskaia EE, Wiercigroch M, Woo K-C, Rodger AA. Modelling of ground moling dynamics by an impact oscillator with a frictional slider. Meccanica 2003;38(1):85–97.
[17] Pavlovskaia EE, Wiercigroch M. Periodic solutions finder for vibro-impact oscillator with a drift. J Sound Vib, in press.
[18] Wiercigroch M. A note on the switch function for the stick-slip phenomenon. J Sound Vib 1994;175:700.
[19] Galvanetto U, Bishop SR. Stick-slip vibrations of a 2-degree-of-freedom geophysical fault model. Int J Mech Sci 1994;36:683.
[20] Nusse HE, Yorke JA. Dynamics: numerical explorations. New York: Springer-Verlag; 1998.
[21] Hsu CS. Cell-to-cell mapping: a method of global analysis for nonlinear systems. New York: Springer-Verlag; 1987.
[22] Soliman MS, Thompson JMT. Integrity measures qualifying the erosion of smooth and fractal basins of attraction. J Sound Vib 1989;135:453–75.